The Astrophysical Journal Letters, 906:L8 (6pp), 2021 January 10 https://doi.org/10.3847/2041-8213/abd318

A Sharp Rise in the Detection Rate of Broad Absorption Line Variations in a Quasar SDSS J141955.26+522741.1

Qinyuan Zhao[1,2], Zhicheng He[1,2], Guilin Liu[1,2], Tinggui Wang[1,2], Hengxiao Guo[3], Lu Shen[1,2], and Guobin Mou[4]
[1] Key laboratory for Research in Galaxies and Cosmology, Department of Astronomy, University of Science and Technology of China, Chinese Academy of Sciences, Hefei, Anhui 230026, People's Republic of China; zcho@ustc.edu.cn, glliu@ustc.edu.cn
[2] School of Astronomy and Space Sciences, University of Science and Technology of China, Hefei, Anhui 230026, People's Republic of China
[3] Department of Physics and Astronomy, 4129 Frederick Reines Hall, University of California, Irvine, CA, 92697-4575, USA
[4] School of Physics and Technology, Wuhan University, Wuhan 430072, People's Republic of China
Received 2020 November 24; revised 2020 December 11; accepted 2020 December 13; published 2021 January 11

Abstract

We present an analysis of the variability of broad absorption lines (BALs) in a quasar SDSS J141955.26+522741.1 at $z = 2.145$ with 72 observations from the Sloan Digital Sky Survey Data Release 16 (SDSS DR16). The strong correlation between the equivalent widths of BALs and the continuum luminosity, reveals that the variation of BAL troughs is dominated by the photoionization. The photoionization model predicts that when the time interval ΔT between two observations is longer than the recombination timescale $t_{\rm rec}$, the BAL variations can be detected. This can be characterized as a "sharp rise" in the detection rate of BAL variation at $\Delta T = t_{\rm rec}$. For the first time, we detect such a "sharp rise" signature in the detection rate of BAL variations. As a result, we propose that the $t_{\rm rec}$ can be obtained from the "sharp rise" of the detection rate of BAL variation. It is worth mentioning that the BAL variations are detected at the time intervals less than the $t_{\rm rec}$ for half an order of magnitude in two individual troughs. This result indicates that there may be multiple components with different $t_{\rm rec}$ but the same velocity in an individual trough.

Unified Astronomy Thesaurus concepts: Broad-absorption line quasar (183); Quasar absorption line spectroscopy (1317); Galaxy winds (626)

1. Introduction

Quasar outflows, as an essential component of the quasar structure, have been considered to play an important role in the coevolution of the central supermassive black holes (SMBHs) and their host galaxies (Silk & Rees 1998; Loeb 2004; Springel et al. 2005; Novak et al. 2011; Soker & Meiron 2011; Choi et al. 2014; Nims et al. 2015; Ciotti et al. 2017). In 10%–40% of quasars with the central source and outflowing gas aligned on the line of sight, outflows may manifest themselves as broad absorption lines (BALs; Weymann et al. 1991; Reichard et al. 2003; Arav et al. 2008; Knigge et al. 2008; Scaringi et al. 2009; Allen et al. 2011). Technically, they are defined as BAL/mini-BALs troughs with velocity widths 2000 km s^{-1} (500–2000 km s^{-1} for mini-BALs) and at depths >10% below the continuum (Weymann et al. 1991; Hamann & Sabra 2004).

It is well known that the BAL troughs are able to vary over timescales from days to years (Capellupo et al. 2011, 2012; Filiz et al. 2012; Arav et al. 2013; Filiz et al. 2013; He et al. 2014, 2015, 2017; Grier et al. 2015; Hemler et al. 2019; Zhang et al. 2015; Shi et al. 2017; Sun et al. 2017; Lu & Lin 2019). Two main mechanisms lead to BAL variations: (1) changes in the ionization of gas and (2) absorbing gas moving in and out of the line of sight. In either case, the BAL variation can provide important clues regarding the origins and the physical conditions of outflows. For case (1), the variability timescale can constrain the recombination timescale of the absorbing gas, which in turn deduces the gas density (Barlow et al. 1992; Wang et al. 2015; He et al. 2019). He et al. (2019) proposed that the fraction curve (i.e., the detection rate; see Section 3 for details) of BAL variation is the integral function of the distribution of recombination timescales. Following this method, for an individual BAL outflow, the fraction curve would be a quasi step function. The recombination timescale would correspond to the time interval at the "sharp rise" of the fraction curve.

In this Letter, we report the first detection of such a "sharp rise" phenomenon of the fraction curve in a BAL quasar SDSS 141955.26+522741.1 at $z = 2.145$ from the SDSS DR16. This object has 72 observations with the signal-to-noise ratio (S/N) level at g band greater than 5 in all the epochs. This object was found to have a strong correlation between the BAL trough and the continuum flux by previous studies (e.g., Hemler et al. 2019; Lu & Lin 2019). The strong correlation and multiple observations make this object an ideal laboratory for the BAL studies. In Section 2, we present the evidence for photoionization-driven BAL variations. In Sections 3 and 4, we measure the fraction curve of BAL variations. The conclusions are in Section 5. Throughout this work, we adopt a standard ΛCDM cosmology with $H_0 = 70$ km s^{-1} Mpc^{-1}, $\Omega_m = 0.3$, and $\Omega_\Lambda = 0.7$.

2. Evidence for Photoionization-driven BAL Variations

2.1. The Spectral Fitting

We adopt the power-law function $f_\lambda = f_{2000}(\lambda/2000)^\alpha$ to fit the continuum of the spectra in the "continuum" windows (shown in Figure 1), which are known to be relatively free from strong emission lines. We use a single Gaussian profile to fit the Si IV and C IV emission lines in the continuum-subtracted spectra. The absorption regions are masked by the visual inspection when fitting emission lines. As shown in Figure 1, a single Gaussian can well fit the emission lines.

The equivalent widths (EW) of the BAL troughs are calculated as follows:

$$\mathrm{EW} = \int C\left[1 - \frac{f_{\rm obs}(\lambda)}{f_{\rm con}(\lambda)}\right] d\lambda, \quad (1)$$

where $f_{\rm obs}$ and $f_{\rm con}$ are the observed flux and power-law continuum flux, respectively, and $C = 1$ at $f_{\rm obs} < f_{\rm con}$, otherwise

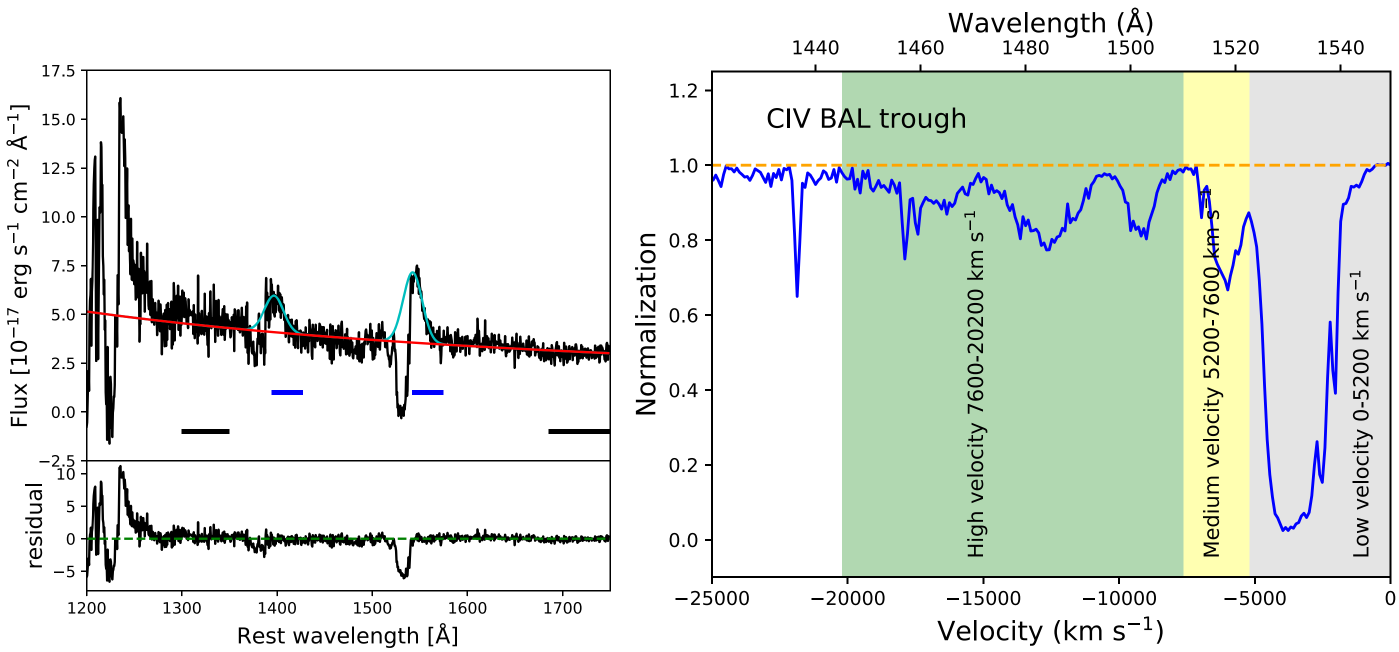

Figure 1. Left panel: An example of the power-law plus Gaussian functions to fit the continuum and emission lines. The black line represents the rest-frame spectrum. The red line is the power-law continuum fitting and the cyan lines are the Gaussian fitting for the Si IV and C IV emission lines. The black and blue horizontal lines are the fitting windows for the continuum and emission lines, respectively. The residual spectrum, i.e., the difference between the observational and model spectrum. Right panel: the normalized composite spectrum for the C IV BAL trough from the 72 observations. We divide the whole trough into three regions: low- (0–5200kms^{-1}, gray), medium- (5200–7600 km s^{-1}, yellow), and high-velocity (7600–20,200 km s^{-1}, green). Due to the low detection rate of BAL variations, the three high-velocity regions are treated as one region.

$C = 0$. According to the normalized composite spectrum (right panel of Figure 1), the BAL trough consists of five components at different velocities (Hemler et al. 2019). We divide the BAL trough into three regions: low- (0–5200 km s^{-1}), medium- (5200–7600 km s^{-1}), and high-velocity (7600–20,200 km s^{-1}). Note that, due to the low detection rate of BAL variations, the three high-velocity regions are treated as one region. The EWs are integrated from 1523 Å to 1550 Å, 1510 Å to 1523 Å, and 1445 Å to 1510 Å for the three regions, respectively. The error for the BAL EW is measured as follows: $\sigma_{\rm EW} = \sqrt{\sum\left(\frac{f_{\rm obs}}{f_{\rm con}}\right)^2\left[\left(\frac{\sigma_{f{\rm obs}}}{f_{\rm obs}}\right)^2 + \left(\frac{\sigma_{f{\rm con}}}{f_{\rm con}}\right)^2\right]}$, where $\sigma_{f_{\rm obs}}$ and $\sigma_{f_{\rm con}}$ are the errors in the observed flux and power-law continuum flux, respectively. We take the luminosity of the fitted power law at 1500 Å (L_{1500}) as the representation of the continuum intensity.

2.2. The Strong Negative Correlation between the BAL EW and the Continuum

The change in the ionization state of an outflow gas can be caused by the variation of the incident ionizing continuum. For a gas in the low ionized state of a specified ion (such C IV), there will be a positive correlation between the C IV column density and the continuum luminosity. In the opposite case, there will be a negative correlation. Same as reported by Hemler et al. (2019) and Lu & Lin (2019), there are strong negative correlations between the BAL EW and the continuum luminosity at 1500 Å for all three regions (see Figure 2). The correlation coefficients and p-values are marked in Figure 2. The strong negative correlations between the BAL troughs and the continuum reveal that the gas is in the overionized state of C IV, and the variation of BAL trough is driven by the variation of ionizing continuum. As a result, this object is an ideal laboratory to analyze the photoionization-driven BAL variations.

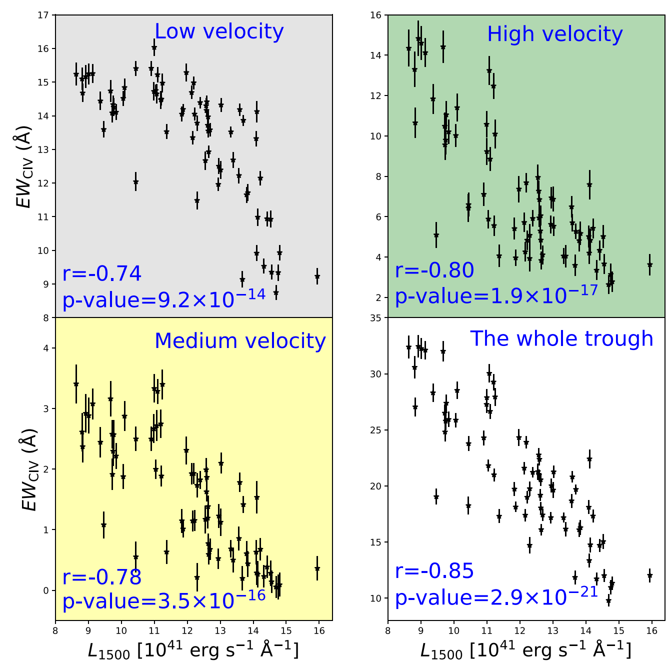

Figure 2. The BAL EW of C IV vs. the luminosity at 1500 Å for three velocity regions as well as the whole BAL. The correlation coefficients and *p*-values are marked in each panel.

3. The Fraction Curve of BAL Variations in an Individual Source

As described in He et al. (2019), the ionization state of a gaseous outflow requires a period of time (the recombination

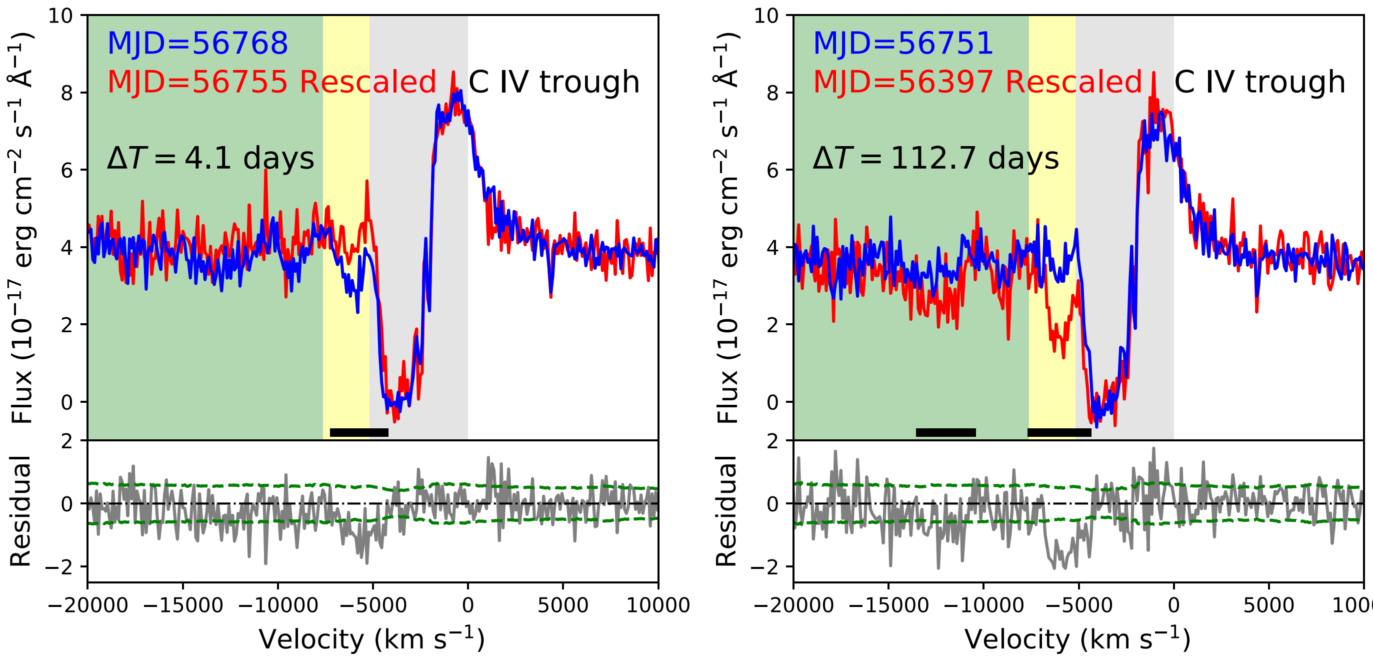

Figure 3. Identification of C IV variable absorption lines. Two examples of matching the reference spectrum (in blue) to another spectrum (in red) by multiplying the reference spectrum with the double power law described in the text. The black horizontal lines represent the varied region of C IV BAL. Left panel is an example of the time interval $\Delta T = 4.1$ days between two observations shorter than the recombination timescale $t_{\rm rec}$ of the low- and medium-velocity regions. Right panel is an example of the time interval $\Delta T = 112.7$ days longer than $t_{\rm rec}$.

timescale, $t_{\rm rec}$, Barlow et al. 1992; Krolik & Kriss 1995; Wang et al. 2015) to respond to changes in the ionizing continuum for the ionized outflows. The gas ionization is connected to the average intensity of the ionizing continuum over $t_{\rm rec}$. We denote the probability of detecting the variability of a BAL with $t_{\rm rec}$ at ΔT as $p(t_{\rm rec}, \Delta T)$. In principle, variability of the absorption line can be detected, only when the time interval (ΔT) between two observations longer than the recombination timescale, i.e., $p = 0$ for $\Delta T < t_{\rm rec}$ and $p = {\rm K}$ (K is a constant greater than 0) for $\Delta T \geqslant t_{\rm rec}$. We define the number ratio of the pair of observations with varied BAL to all the pairs of observations as the $F(\Delta T)$. As shown in Equation (1) in He et al. (2019), the fraction $F(\Delta T)$ can be written as the integral function of the distribution of recombination timescale $f(t_{\rm rec})$:

$$F(\Delta T) = \int_0^{+\infty} p(t_{\rm rec}, \Delta T) f(t_{\rm rec}) dt_{\rm rec} = {\rm K} \int_0^{\Delta T} f(t_{\rm rec}) dt_{\rm rec}. \quad (2)$$

For an individual source, the $t_{\rm rec}$ is a single value. The distribution of recombination timescale $f(t)$ is a δ function: $f(t) = 0\ (t \neq t_{\rm rec})$ and $\int_{-\infty}^{+\infty} f(t) dt = 1$. As a result, the $F(\Delta T)$ is a step function:

$$F(\Delta T) = \begin{cases} 0, & \Delta T < t_{\rm rec} \\ {\rm K}({\rm K} > 0), & \Delta T \geqslant t_{\rm rec}. \end{cases} \quad (3)$$

In the actual observations, the $F(\Delta T)$ is a quasi step function and the measured $t_{\rm rec}$ is a Gaussian function with a certain width. So, it is expected that there will be a "sharp rise" phenomenon in the measured $F(\Delta T)$ curve around $\Delta T = t_{\rm rec}$.

4. The Observed Fraction Curve of BAL Variations

4.1. Identification of the Variable Regions in BAL Troughs

We follow the same method as He et al. (2019) to identify the variable region of the BAL trough. As described in the Methods section of He et al. (2019), we take two main steps to identify the variation region of BAL troughs between a pair of spectra. (1) We select the higher S/N spectrum of the pair of spectra as a template to match the other spectra by rescaling it using the double power-law function (Equation (1) in Wang et al. 2015) to account for the potential variations of the continuum shape. Then, we add/subtract a Gaussian to/from the rescaled spectrum to account for variations of the emission line. As shown in Figure 3, the rescaled template matching produces a better fit outside the absorption line region. As a result, we measure the absorption line variability from the difference spectrum. (2) We search the difference spectrum for the contiguous negative and positive pixels and mark all pixels where the difference is greater than 3σ. Adjacent marked pixels are then connected to form a variable region. Then we expand such regions into neighboring pixels that have the same sign in the difference spectrum but lie at the less than 3σ significance level. Finally, we merge the neighboring regions with the same variable sign and with a separation of less than four pixels (about 1.5 Å, corresponding to 300 km s^{-1}). Due to the low S/N in the Si IV region, we only carry on the identification for C IV BALs. As shown in Figure 4, the 72 observations of SDSS J141955.26+522741.1 yield 2556 spectral pairs. The amplitude of continuum variation at 1500 Å between a pair of observations is defined as follows:

$$\frac{\Delta L}{L} = 2\frac{L_2 - L_1}{L_2 + L_1}, \quad (4)$$

where the L_1 and L_2 are the flux of the pair of observations. The amplitudes of continuum variations $|\Delta L/L|$ can affect the BAL

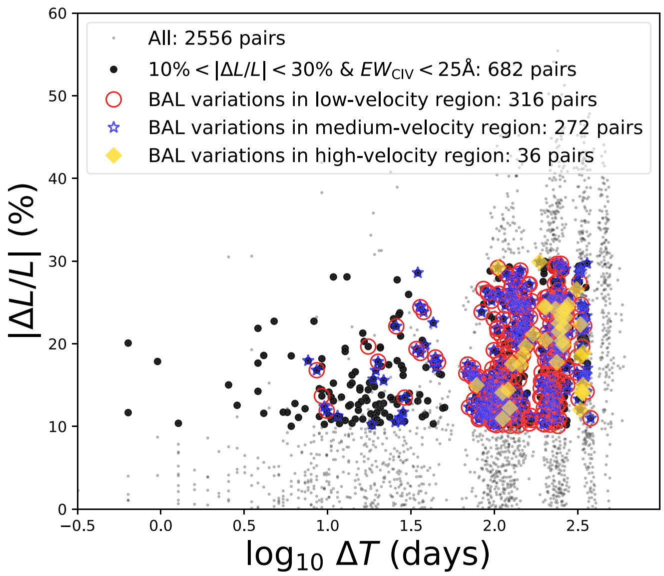

Figure 4. The data selection. The 72 observations of SDSS J141955.26+522741.1 yield 2556 spectral pairs (gray points). To ensure the amplitudes of continuum variations are similar in different time intervals, we cut the $|\Delta L/L|$ between 10% and 30%. To reject the deep absorption, we select the mean value of C IV BAL EW in each pair of spectra to smaller than 25 Å. After the above screening, there are 682 pairs of spectra retained (black points). In the 682 pairs of spectra, the number of pairs detected to have BAL variations are 316, 272, and 36 for the low- (red circles), medium- (blue stars), and high-velocity (yellow squares) regions, respectively.

variability. So, we cut the $|\Delta L/L|$ between 10% and 30% to ensure the $|\Delta L/L|$ are similar in different time intervals. The variation of BAL is difficult to detect when the BAL trough is deep (also a low S/N of flux) or saturated. So, we cut the mean value of C IV BAL EW in each pair of spectra to smaller than 25 Å to reject the deep absorption. This action also reduces the difference of BAL EW between different time intervals. As shown in Figure 4, after this screening, there are 682 pairs of spectra retained. In the 682 pairs of spectra, the number of pairs detected to have BAL variations are 316, 272, and 36 for the low-, medium-, and high-velocity regions, respectively.

4.2. Measuring the Fraction F(ΔT) *Curve*

To measure the $F(\Delta T)$, we sorted these 682 pairs by the rest time interval between each pair of observations and divided among 8 bins. Each of the first three bins has 50 spectral pairs. Each of the next four bins has 100 spectral pairs. The last interval has 132 spectral pairs. For the ith bin, the fraction $F_i(\Delta T_i)$ is measured to be $F_i = k_i/N_i$, where ΔT_i is the mean time interval of spectral pairs, k_i is the number of spectral pairs with variable BAL, N_i is the number of all spectral pairs in the ith bin. Since the estimation of F_i amounts to an N_i-fold Bernoulli trial, one can use $\sigma_{F_i} = \sqrt{F_i(1 - F_i)/N_i}$ as an estimate of the measurement error of F_i. The measured fraction curve is shown in Figure 5. As predicted, there is an obvious "sharp rise" signature in the fraction curve for the low- and medium-velocity regions of the C IV BAL. In addition, there is a "weak rise" signature in the fraction curve of the high-velocity region. The fraction curve shows two phases. The value of $F(\Delta T)$ at $\log_{10}\Delta T < 1.5$ is significantly lower that at $\log_{10}\Delta T > 1.5$ in the fraction curve for the low- and medium-velocity regions.

Assuming that the error of $t_{\rm rec}$ is a Gaussian function, the fraction $F(\Delta T)$ curve is the cumulative distribution function (CDF) of the Gaussian distribution:

$$F(t) = p_0\left[1 + \mathrm{erf}\left(\frac{t - p_1}{\sqrt{2}\,p_2}\right)\right], \quad (5)$$

where $t \equiv \log_{10}\Delta T$ is the logarithmic time interval of the spectral pair, $\mathrm{erf}(t) = 1\big/\sqrt{\pi}\int_{-t}^{t} e^{-x^2}dx$ is the error function, and $p_1 = t_c$, $p_2 = t_\sigma$, i.e., the mean and standard deviation of the Gaussian distribution, respectively. The best-fit recombination timescale of C IV is $t_{\rm rec} = 10^{1.57\pm0.16}$ and $10^{1.29\pm0.03}$ days for the low- and medium-velocity regions, respectively.

As shown in the bottom panels of Figure 5, the BAL EWs gradually increase in the last five bins. Due to the deep absorption of the low-velocity region, the detection rate decreases as the BAL EW increases. The absorptions in the medium- and high-velocity regions are not deep or saturated. As a result, the detection rate does not decrease as the BAL EW increases (shown in panels (d) and (g)).

4.3. Multiple Components with Different Recombination Timescales in a Single Trough?

As shown in Figures 3 and 4, the BAL variations in the low- and medium-velocity regions can be detected at $\Delta T < 10^{1.0}$ days. Furthermore, as shown in panels (a) and (d) of Figure 5, the fraction $F(\Delta T)$ of the low- and medium-velocity regions is 6% (3/50) and 10% (5/50) at $\Delta T = 10^{0.8}$ days, respectively. However, the deduced recombination timescales are $t_{\rm rec} = 10^{1.57\pm0.16}$ and $10^{1.29\pm0.03}$ days for the low- and medium-velocity regions, respectively. As a result, the BAL variations are detected at the time intervals less than the $t_{\rm rec}$ for half an order of magnitude. This result indicates that there may be another component with a shorter recombination timescale in these two individual troughs. More observations at shorter time intervals are needed to determine at what timescale the detection rate falls to near zero.

In addition, the low detection rate of BAL variation prevents us from extracting the recombination timescale in the high-velocity region. There is only a "weak rise" between $\Delta T = 10^{1.5}$ and $10^{2.5}$ days in the high-velocity region. More observations with longer intervals are also needed to improve the statistical significance of the "weak rise" signature.

5. Conclusions

In this work, we analyze the BAL variations in SDSS J141955.26+522741.1, a BAL quasar at $z = 2.145$ with 72 observations from the SDSS DR16. The strong correlations between the BAL troughs and the continuum allow us to analyze the photoionization-driven BAL variations. Our results can be summarized as follows:

1. As predicted by Barlow et al. (1992), Krolik & Kriss (1995), Wang et al. (2015), and He et al. (2019), the detection rate of BAL variations is a quasi step function. For the first time, we detect an obvious "sharp rise" signature in the fraction curve of C IV BAL variations of two individual velocity components. The recombination timescale of C IV deduced from the fraction curve is $t_{\rm rec} = 10^{1.57\pm0.16}$ and $10^{1.29\pm0.03}$ days for the low- and medium-velocity regions, respectively. In addition, there

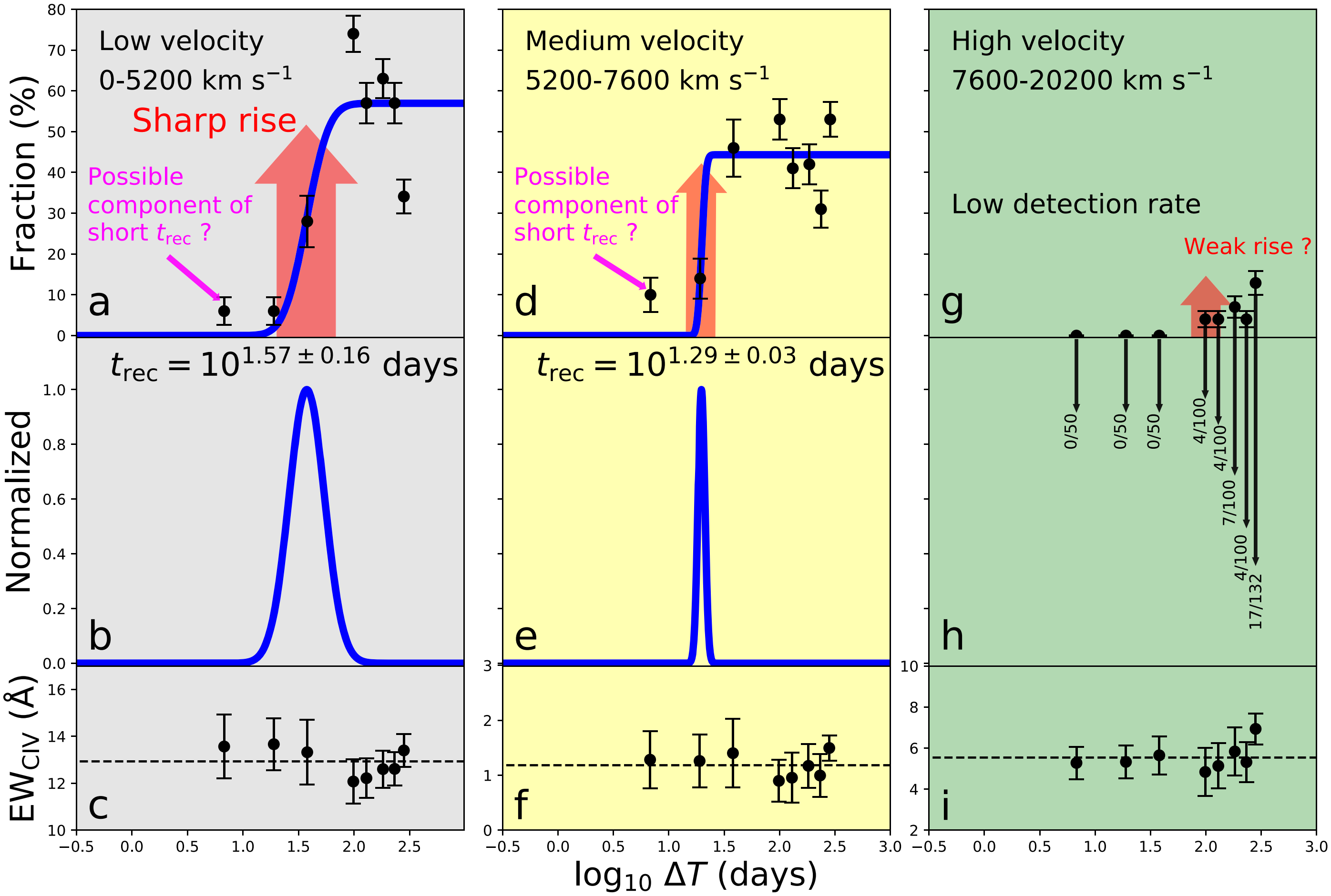

Figure 5. The fraction curve of BAL variations of C IV in SDSS J141955.26+522741.1. For the first time, we detect a "sharp rise" signature in the fraction curve of the low- and medium-velocity regions (panels (a) and (d)), and a "weak rise" signature in the high-velocity region (panel (g)). The cumulative distribution function of a Gaussian distribution is used to model the fraction curve. Panels (b) and (e): the deduced recombination timescales are $t_{rec} = 10^{1.57 \pm 0.16}$ and $10^{1.29 \pm 0.03}$ days for the low- and medium-velocity regions, respectively. The BAL variations are detected at the time intervals less than t_{rec} for half an order of magnitude. This result indicates that there may be another component with a shorter recombination timescale in these two individual troughs. Panels (c), (f), and (i): the mean and standard deviation of BAL EWs for all the spectral pairs in each bin. The horizontal dashed line is the mean value of BAL EWs for all spectral pairs. Due to the deep absorption of the low-velocity region, the detection rate decreases as the BAL EW increases in the last five bins. The absorptions in the medium- and high-velocity regions are not deep or saturated. As a result, the detection rate does not decrease as the BAL EW increases.

is a "weak rise" between $\Delta T = 10^{1.5}$ and $10^{2.5}$ days in the high-velocity region. More observations with longer intervals are needed to improve the statistical significance of the "weak rise" signature.

2. In the low- and medium-velocity troughs, the BAL variations are detected at the time intervals less than the t_{rec} for half an order of magnitude. This result indicates that there may be another component with a shorter recombination timescale in the individual trough. However, the statistical significance of current data is insufficient to confirm this conclusion. In the future, more observations at short time intervals may reveal the answer.

We thank the anonymous referee for valuable comments and constructive suggestions. Z.-C.H. is supported by NSFC-11903031 and USTC Research Funds of the Double First-Class Initiative YD 3440002001. G.-L.L. acknowledges the grant from the National Natural Science Foundation of China (No. 11673020 and No. 11421303) and the Ministry of Science and Technology of China (National Key Program for Science and Technology Research and Development, No. 2016YFA0400700). H.-X.G. acknowledges the NSF grant AST-1907290. G.M. acknowledges the Fundamental Research Funds for the Central Universities (No. 2042019kf0040). This work is also supported by NSFC (11833007 and 11703022).

Funding for the Sloan Digital Sky Survey IV has been provided by the Alfred P. Sloan Foundation, the U.S. Department of Energy Office of Science, and the Participating Institutions.

SDSS-IV acknowledges support and resources from the Center for High Performance Computing at the University of Utah. The SDSS website is www.sdss.org.

SDSS-IV is managed by the Astrophysical Research Consortium for the Participating Institutions of the SDSS Collaboration including the Brazilian Participation Group, the Carnegie Institution for Science, Carnegie Mellon University, Center for Astrophysics|Harvard & Smithsonian, the Chilean Participation Group, the French Participation Group, Instituto de Astrofísica de Canarias, The Johns Hopkins University, Kavli Institute for the Physics and Mathematics of the Universe (IPMU)/University of Tokyo, the Korean Participation Group, Lawrence Berkeley National Laboratory, Leibniz Institut für Astrophysik Potsdam (AIP), Max-Planck-Institut für Astronomie (MPIA Heidelberg), Max-Planck-Institut für Astrophysik (MPA Garching), Max-

Planck-Institut für Extraterrestrische Physik (MPE), National Astronomical Observatories of China, New Mexico State University, New York University, University of Notre Dame, Observatário Nacional/MCTI, The Ohio State University, Pennsylvania State University, Shanghai Astronomical Observatory, United Kingdom Participation Group, Universidad Nacional Autónoma de México, University of Arizona, University of Colorado Boulder, University of Oxford, University of Portsmouth, University of Utah, University of Virginia, University of Washington, University of Wisconsin, Vanderbilt University, and Yale University.

ORCID iDs

Zhicheng He https://orcid.org/0000-0003-3667-1060
Guilin Liu https://orcid.org/0000-0003-2390-7927
Tinggui Wang https://orcid.org/0000-0002-1517-6792
Hengxiao Guo https://orcid.org/0000-0001-8416-7059
Lu Shen https://orcid.org/0000-0001-9495-7759
Guobin Mou https://orcid.org/0000-0002-0092-7944

References

Allen, J. T., Hewett, P. C., Maddox, N., Richards, G. T., & Belokurov, V. 2011, MNRAS, 410, 860
Arav, N., Borguet, B., Chamberlain, C., Edmonds, D., & Danforth, C. 2013, MNRAS, 436, 3286
Arav, N., Moe, M., Costantini, E., et al. 2008, ApJ, 681, 954
Barlow, T. A., Junkkarinen, V. T., Burbidge, E. M., et al. 1992, ApJ, 397, 81
Capellupo, D. M., Hamann, F., Shields, J. C., Rodríguez Hidalgo, P., & Barlow, T. A. 2011, MNRAS, 413, 908
Capellupo, D. M., Hamann, F., Shields, J. C., Rodríguez Hidalgo, P., & Barlow, T. A. 2012, MNRAS, 422, 3249
Choi, E., Naab, T., Ostriker, J. P., Johansson, P. H., & Moster, B. P. 2014, MNRAS, 442, 440
Ciotti, L., Pellegrini, S., Negri, A., & Ostriker, J. P. 2017, ApJ, 835, 15
Filiz, Ak, N., Brandt, W. N., Hall, P. B., et al. 2012, ApJ, 757, 114
Filiz, Ak, N., Brandt, W. N., Hall, P. B., et al. 2013, ApJ, 777, 168
Grier, C., Hall, P., Brandt, W., et al. 2015, ApJ, 806, 111
Hamann, F., & Sabra, B. 2004, in ASP Conf. Ser. 311, AGN Physics with the Sloan Digital Sky Survey, ed. G. T. Richards & P. B. Hall (San Francisco, CA: ASP), 203
He, Z., Wang, T., Liu, G., et al. 2019, NatAs, 3, 265
He, Z., Wang, T., Zhou, H., et al. 2017, ApJS, 229, 22
He, Z.-C., Bian, W.-H., Ge, X., & Jiang, X.-L. 2015, MNRAS, 454, 3962
He, Z.-C., Bian, W.-H., Jiang, X.-L., & Wang, Y.-F. 2014, MNRAS, 443, 2532
Hemler, Z., Grier, C., Brandt, W., et al. 2019, ApJ, 872, 21
Knigge, C., Scaringi, S., Goad, M. R., & Cottis, C. E. 2008, MNRAS, 386, 1426
Krolik, J. H., & Kriss, G. A. 1995, ApJ, 447, 512
Loeb, A. 2004, MNRAS, 350, 725
Lu, W.-J., & Lin, Y.-R. 2019, ApJ, 883, 30
Nims, J., Quataert, E., & Faucher-Giguère, C.-A. 2015, MNRAS, 447, 3612
Novak, G. S., Ostriker, J. P., & Ciotti, L. 2011, ApJ, 737, 26
Reichard, T. A., Richards, G. T., Schneider, D. P., et al. 2003, AJ, 125, 1711
Scaringi, S., Cottis, C. E., Knigge, C., & Goad, M. R. 2009, MNRAS, 399, 2231
Shi, X.-H., Pan, X., Zhang, S.-H., et al. 2017, ApJL, 843, L14
Silk, J., & Rees, M. J. 1998, A&A, 331, L1
Soker, N., & Meiron, Y. 2011, MNRAS, 411, 1803
Springel, V., Di Matteo, T., & Hernquist, L. 2005, MNRAS, 361, 776
Sun, L., Zhou, H., Ji, T., et al. 2017, ApJ, 838, 88
Wang, T., Yang, C., Wang, H., & Ferland, G. 2015, ApJ, 814, 150
Weymann, R. J., Morris, S. L., Foltz, C. B., & Hewett, P. C. 1991, ApJ, 373, 23
Zhang, S., Zhou, H., Shi, X., et al. 2015, ApJ, 815, 113